

FILE COPY

(4)

REPORT SD-TR-89-44

AD-A210 502

# High Energy Neutron Irradiation Effects in GaAs Modulation-Doped Field Effect Transistors (MODFETS): Threshold Voltage

Prepared by

R. J. KRANTZ, W. L. BLOSS, and M. J. O'LOUGHLIN  
Electronics Research Laboratory  
Laboratory Operations  
The Aerospace Corporation  
El Segundo, CA 90245

15 June 1989

Prepared for

SPACE SYSTEMS DIVISION  
AIR FORCE SYSTEMS COMMAND  
Los Angeles Air Force Base  
P.O. Box 92960  
Los Angeles, CA 90009-2960

DTIC  
ELECTE  
JUL 24 1989  
S E D

APPROVED FOR PUBLIC RELEASE;  
DISTRIBUTION UNLIMITED

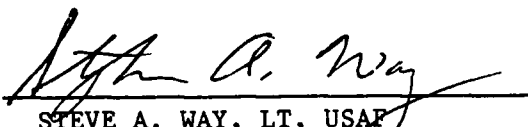
89 7 24 082


This report was submitted by The Aerospace Corporation, El Segundo, CA 90245, under Contract No. F04701-88-C-0089 with the Space Systems Division, P.O. Box 92960, Los Angeles, CA 90009-2960. It was reviewed and approved for The Aerospace Corporation by M. J. Daugherty, Director, Electronics Research Laboratory.

Lt Steve Way was the project officer for the Mission-Oriented Investigation and Experimentation (MOIE) Program.

This report has been reviewed by the Public Affairs Office (PAS) and is releasable to the National Technical Information Service (NTIS). At NTIS, it will be available to the general public, including foreign nationals.

This technical report has been reviewed and is approved for publication. Publication of this report does not constitute Air Force approval of the report's findings or conclusions. It is published only for the exchange and stimulation of ideas.

  
STEVE A. WAY, LT, USAF  
MOIE Project Officer  
AFSTC/WCO OL-AB

  
JAMES A. BERES, LT COL, USAF  
MOIE Program Manager  
AFSTC/WCO OL-AB

## REPORT DOCUMENTATION PAGE

1a. REPORT SECURITY CLASSIFICATION <b>Unclassified</b>			1b. RESTRICTIVE MARKINGS		
2a. SECURITY CLASSIFICATION AUTHORITY			3. DISTRIBUTION/AVAILABILITY OF REPORT  Approved for public release; distribution unlimited.		
2b. DECLASSIFICATION/DOWNGRADING SCHEDULE					
4. PERFORMING ORGANIZATION REPORT NUMBER(S)  TR-0089(4925-07)-3			5. MONITORING ORGANIZATION REPORT NUMBER(S)  SD-TR-89-44		
6a. NAME OF PERFORMING ORGANIZATION The Aerospace Corporation Laboratory Operations		6b. OFFICE SYMBOL (If applicable)		7a. NAME OF MONITORING ORGANIZATION Space Division	
6c. ADDRESS (City, State, and ZIP Code)  El Segundo, CA 90245			7b. ADDRESS (City, State, and ZIP Code)  Los Angeles Air Force Base Los Angeles, CA 90009-2960		
8a. NAME OF FUNDING/SPONSORING ORGANIZATION		8b. OFFICE SYMBOL (If applicable)		9. PROCUREMENT INSTRUMENT IDENTIFICATION NUMBER  F04701-88-C-0089	
8c. ADDRESS (City, State, and ZIP Code)			10. SOURCE OF FUNDING NUMBERS		
			PROGRAM ELEMENT NO.	PROJECT NO.	TASK NO.
			WORK UNIT ACCESSION NO.		
11. TITLE (Include Security Classification) High Energy Neutron Irradiation Effects in GaAs Modulation-Doped Field Effect Transistors (MODFETS): Threshold Voltage					
12. PERSONAL AUTHOR(S) Krantz, R. J., Bloss, W. L., and O'Loughlin, M. J.					
13a. TYPE OF REPORT		13b. TIME COVERED FROM _____ TO _____		14. DATE OF REPORT (Year, Month, Day) 1989 June 15	
				15. PAGE COUNT 33	
16. SUPPLEMENTARY NOTATION.					
17. COSATI CODES			18. SUBJECT TERMS (Continue on reverse if necessary and identify by block number)		
FIELD	GROUP	SUB-GROUP			
			Neutron degradation		
			Neutron fluence		
			Fermi level		
			Amphoteric traps		
19. ABSTRACT (Continue on reverse if necessary and identify by block number)					
<p>The effects of high energy neutrons of fluences approaching <math>1 \times 10^{15} \text{ cm}^{-2}</math> on MODFETs have been studied. Neutron-induced threshold voltage shifts are described by application of a finite temperature strong inversion, depletion layer, charge control model. The results of this model show that the neutron-induced threshold voltage is a consequence of electron trapping in the GaAs layer near the AlGaAs/GaAs interface. This allows a convenient parameterization of the neutron degradation by accounting for these trapped electrons as "effective acceptors", defining an effective acceptor introduction rate, and applying the charge control model to describe the threshold voltage. Our analysis shows that neutron degradation in these AlGaAs/GaAs heterostructures is dominated by the change in the depletion layer charge and the shift in the Fermi level with neutron fluence. The dominant mechanisms are shown to depend on GaAs material parameters, only. The contribution due to the AlGaAs layer carrier removal is &lt;3% of the total threshold voltage shift.</p>					
20. DISTRIBUTION/AVAILABILITY OF ABSTRACT			21. ABSTRACT SECURITY CLASSIFICATION		
<input checked="" type="checkbox"/> UNCLASSIFIED/UNLIMITED <input type="checkbox"/> SAME AS RPT <input type="checkbox"/> DTIC USERS			Unclassified		
22a. NAME OF RESPONSIBLE INDIVIDUAL			22b. TELEPHONE (Include Area Code)		22c. OFFICE SYMBOL

# PREFACE

We would like to thank B. K. Janousek, W. E. Yamada, and L. W. Aukerman for their technical assistance in this study.

Accession For	
NTIS CRA&I	<input checked="" type="checkbox"/>
DTIC TAB	<input type="checkbox"/>
Unannounced	<input type="checkbox"/>
Justification	
By	
Distribution	
Availability Codes	
Dist	Avail and/or Special
A-1	



## CONTENTS

I.	BACKGROUND.....	5
	A. Structure.....	5
	B. Threshold Voltage Definition.....	6
II.	NEUTRON-INDUCED THRESHOLD VOLTAGE SHIFTS.....	11
	A. Neutron-Induced Trap Levels and Charge Densities.....	11
	B. Threshold Voltage Shift.....	14
	C. Low Fluence Expansion.....	17
III.	EXPERIMENTAL COMPARISON.....	19
IV.	DISCUSSION.....	23
V.	SUMMARY.....	27
	REFERENCES .....	29
	APPENDIX A - (Fermi Level and $n_s$ ).....	31
	APPENDIX B - ( $E_o$ and $n_s$ ).....	33
	APPENDIX C - ( $n_{th}$ , $N_a$ , and $W$ ).....	35

## FIGURES

1.	Pre-irradiation Band Diagram of a Typical MODFET Structure with Schottky Contact, $\phi_m$ , Under Bias, $V_g$ .....	6
2.	Post-irradiation Band Diagram of a Typical MODFET Structure.....	12
3.	Stylized Version of the MODFET Structure Used in This Study.....	20
4.	Change in Threshold Voltage vs Neutron Fluence for the Model Parameters Shown.....	21
5.	Threshold Voltage vs Neutron Fluence Using the Model Parameters Used to Fit the Threshold Shift Data.....	22
6.	Contributions to the Threshold Voltage Shift vs Neutron Fluence.....	22
7.	MODFET Energy Bands Near the Interface Pre-(i) and Post-(f) Neutron Irradiation.....	24
8.	Energy of the Quantum Well Level and the Fermi Level vs Neutron Fluence.....	24
9.	Change in the Quantum Well Level and the Fermi Level vs Neutron Fluence.....	25
10.	Depletion Layer Width vs Neutron Fluence.....	25

## I. BACKGROUND

$\text{Al}_x\text{Ga}_{1-x}\text{As}/\text{GaAs}$  MODFETs have become increasingly important in III-V semiconductor device circuit development.<sup>1</sup> Although most significant at cryogenic temperatures, speed and power advantages over GaAs MESFET technologies are evident even at room temperature.<sup>2</sup> In applications where epitaxial growth is necessary, such as GaAs on Si, there is no impediment to the use of these devices. As GaAs MODFETs are being developed for a variety of high-speed analog (>60 GHz) and digital (200 MHz clock rate) spaced-based systems,<sup>3,4</sup> an understanding of the radiation degradation of these devices is of particular importance.

In an attempt to understand the results of neutron testing of Aerospace fabricated MODFETs we have developed a charge control, depletion layer model for neutron-induced threshold voltage shifts in AlGaAs/GaAs heterojunction devices. In the following subsection we review the salient features of MODFET band structure. The subsequent subsection contains a lengthy summary of the threshold voltage results of our MODFET strong inversion model, which has been discussed elsewhere.<sup>5</sup>

Section II contains the details of the model used to describe neutron degradation in these structures, and how the neutron-induced threshold voltage shifts are derived. In Section III, experimental results for the neutron-induced threshold voltage shifts are compared with the analytical results derived in Section II.

### A. STRUCTURE

The band structure of a typical<sup>6</sup> AlGaAs(n)/GaAs heterojunction with a Schottky gate, under bias, is shown in Fig. 1. The wide bandgap AlGaAs layer of thickness (a+d) lies between the gate and the narrow bandgap GaAs layer. The mismatch between the bandgaps causes the formation of a two-dimensional quantum well at the AlGaAs/GaAs interface. The doped AlGaAs layer of thickness d is separated from the two-dimensional channel by a spacer layer of thickness a. Doping concentrations in the AlGaAs(n) layer

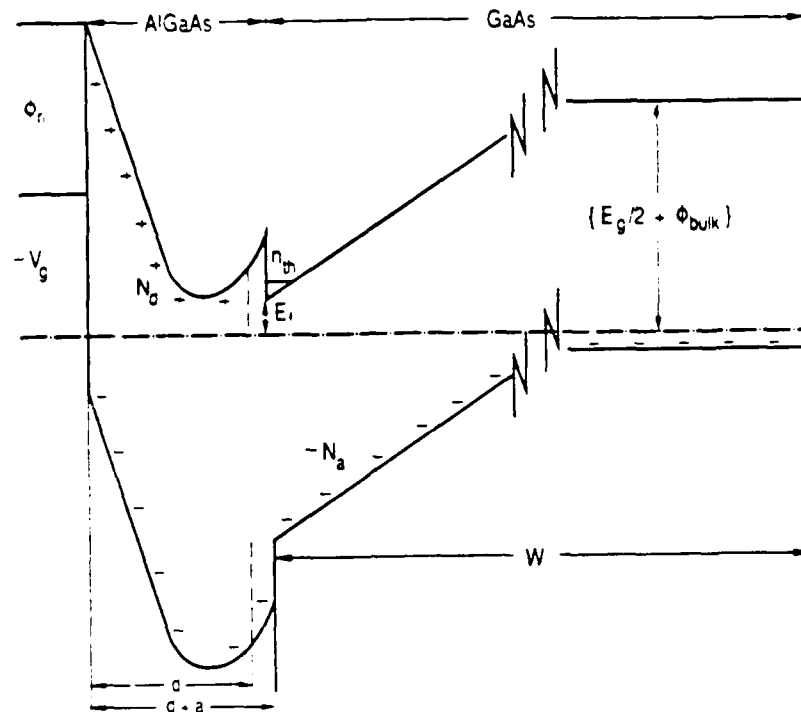


Fig. 1. Pre-irradiation Band Diagram of a Typical MODFET Structure with Schottky Contact,  $\phi_m$ , Under Bias,  $V_g$ . AlGaAs donors and unintentional acceptors are assumed to be completely ionized. Near threshold the Fermi level (dashed line) lies below the bottom of the 2-D well.

are on the order of  $10^{18} \text{ cm}^{-3}$  and are the source of mobile carriers. Because the 2-D channel is separated from the highly doped AlGaAs(n) region and the "unintentional" acceptor doping concentrations in the GaAs are low, typically  $10^{13} - 10^{15} \text{ cm}^{-3}$  for molecular beam epitaxy (MBE) processed devices, enhanced mobilities are achieved (particularly at low temperatures) due primarily to reduced impurity scattering.<sup>7</sup>

#### B. THRESHOLD VOLTAGE DEFINITION

In the depletion layer approximation under the conditions depicted in Fig. 1, it can be shown by application of Gauss's law across the that the field at the AlGaAs/GaAs interface is

$$E_i = (-V_{\text{off}} - E_f + V_g)/(d + a) \quad (1)$$



where

- $V_{\text{off}}$  = the voltage which "annihilates" the channel charge
- $E_f$  = the Fermi level relative to the bottom of the well
- $V_g$  = applied gate voltage
- $d$  = the doped AlGaAs(n) layer thickness
- $a$  = the spacer layer thickness.

The term  $V_{\text{off}}$  is given by

$$V_{\text{off}} = \phi_m - \Delta E_c - V_{A1} \quad (2)$$

where

- $\phi_m$  = the Schottky barrier height
- $\Delta E_c$  = the conduction band offset
- $V_{A1}$  = the voltage drop across the AlGaAs layer.

For an AlGaAs donor density of  $N_d$  in the depletion layer approximation, the voltage drop across the AlGaAs layer is

$$V_{A1} = -qN_d d^2 / 2\epsilon \text{ (minus the pinch-off voltage, } V_p) \quad (3)$$

where

- $q$  = the electronic charge
- $\epsilon$  = the AlGaAs permittivity (assumed to be identical to the GaAs permittivity in what follows).

Substituting Eqs. (2) and (3) into Eq. (1) we may write

$$V_g' = V_{A1} + (d + a)E_i + E_f \quad (4)$$

where

$$V_g' = V_g - \phi_m + E_c.$$

In the neutron degradation analysis that follows, the Schottky barrier height and the conduction band offset are unaffected. It is convenient, therefore, to consider only  $V_g'$ .

In Appendix A we show that the Fermi level,  $E_f$ , depends on the channel density,  $n_s$ , in the following way:

$$E_f = E_0 + (kT/q) \ln(C_2 n_s / (kT/q)) \quad (5)$$

where

$E_0$  = the first quantum level in the 2-D well

$kT/q$  = the absolute temperature in volts

$N_a$  = the unintentional acceptor doping density

$W$  = the GaAs depletion layer width.

As shown in Appendix B the first quantum level may be written as

$$E_0 = C_1 (n_s + N_a W)^{2/3} \quad (6)$$

In MODFETs we take threshold to occur at strong inversion when the channel carrier density,  $n_s$ , is equal to the local acceptor density,  $N_a$ , times the average width of the two-dimensional channel,  $z_{ave}$ . Thus,

$$n_{th} = N_a z_{ave} \quad (7)$$

This relationship for the channel density at threshold is consistent with the strong inversion definition of threshold in MOSFETs. In that case, strong inversion occurs when the density of electrons in the channel

is equal to the density of acceptors in the bulk. Our definition is the two-dimensional analog. The consequences of this definition are discussed in more detail elsewhere.<sup>5</sup> In Appendix C we show that the channel density in the single subband triangular well approximation at threshold is related to the depletion layer width in the following way:

$$n_{th} = C_0(N_a)^{2/3}/W^{1/3} \quad (8)$$

Substitution of Eqs. (5), (6), (7), and (8) into Eq. (4) yields  $V_g'$  at threshold in terms of the AlGaAs(n) doping density,  $N_d$ , the acceptor doping density,  $N_a$ , the depletion width,  $W$ , and appropriate geometrical factors. As in the case for MOSFETs, the depletion width is related to the band bending in the bulk,  $\phi_{BB}$ , by

$$W = [2(\epsilon/q)\phi_{BB}/N_a]^{1/2} \quad (9)$$

With the help of Fig. 1, the band bending is shown to be:

$$\phi_{BB} = E_g/2 + \phi_{bulk} - E_f \quad (10)$$

where

$E_g$  = the GaAs bandgap

$\phi_{bulk}$  = the GaAs bulk potential [ $\sim (kT/q)\ln(N_a/n_i)$ ] ( $n_i$  is the GaAs intrinsic carrier density  $\sim 10^6 \text{ cm}^{-3}$  at room temperature)

This result for the band bending in MODFETs is slightly different than that for MOSFETs and is discussed elsewhere.<sup>5</sup> With the use of Eqs. (9) and (10),  $V_g'$  at threshold, which we will write as  $V_{th}'$ , depends only on the doping densities and the geometry.

Application of Gauss's law from the interface to the edge of the depletion layer yields the field at the interface in terms of GaAs doping only. Inspection of Eq. (4) shows that the contribution to the threshold voltage by the AlGaAs material parameters and the GaAs material parameters may be separated and examined independently. This property of the threshold voltage will be exploited when the neutron-induced threshold voltage results are discussed.

## II. NEUTRON-INDUCED THRESHOLD VOLTAGE SHIFTS

After neutron irradiation and at threshold, Eq. (4) may be rewritten to reflect the post-irradiation value of  $V_{th}'$  thus

$$V_{th}'' = V_{Al}'' + (d + a)E_i'' + E_f'' \quad (11)$$

where double primes (") indicate the post-irradiation values. The difference between the pre-irradiation value,  $V_{th}'$ , and  $V_{th}''$  is the neutron-induced threshold voltage shift, or

$$\Delta V_{th} = \Delta V_{Al} + (d + a)\Delta E_i + \Delta E_f. \quad (12)$$

In the following subsection the model which describes the redistribution of charges due to neutron bombardment is described. The subsequent subsection contains a discussion of threshold voltage shifts due to each of the terms in Eq. (12).

### A. NEUTRON-INDUCED TRAP LEVELS AND CHARGE DENSITIES

It is well known that high energy neutron bombardment of semiconductors introduces deep traps in the bandgap of the material.<sup>8,9</sup> In lieu of any detailed knowledge of the exact location of these traps, we assume that the neutron-induced trap may be described as an effective amphoteric trap located at midgap. This assumption reflects experimental results which show that neutron bombardment of both p and n type material results in the material becoming more intrinsic.<sup>10-13</sup> Making this assumption for both the AlGaAs and the GaAs, the MODFET band diagram after neutron irradiation may be depicted as shown in Fig. 2. Amphoteric traps located below the Fermi level charge negatively whereas traps above the Fermi level charge positively. As a result, the voltage drop across the AlGaAs,  $V_{Al}$ , the field at the interface,  $E_i$ , and the Fermi level,  $E_f$ , at threshold will change with neutron irradiation.

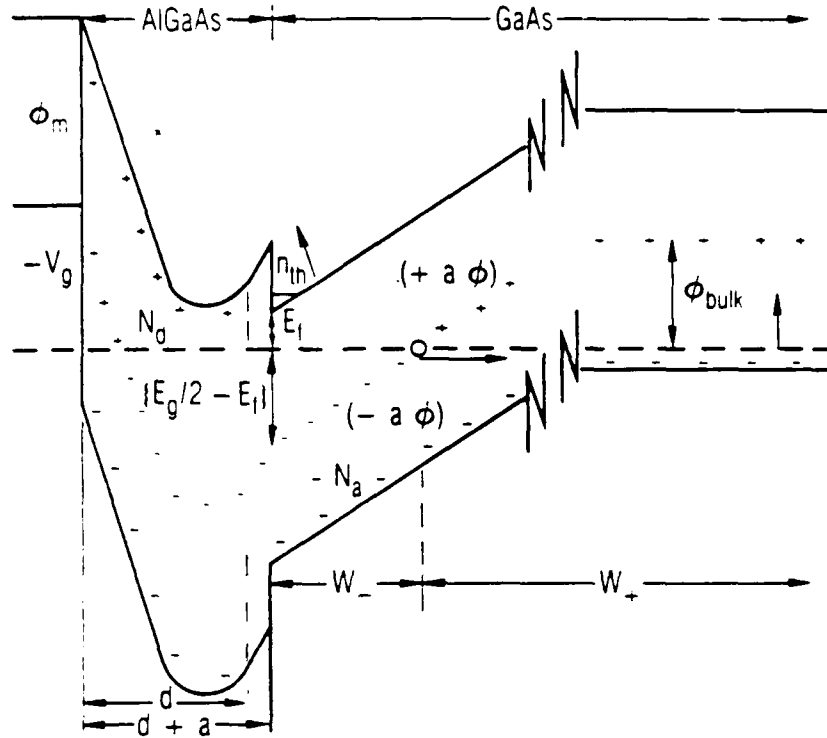


Fig. 2. Post-irradiation Band Diagram of a Typical MODFET Structure. Effective amphoteric midgap traps charge negatively when below the Fermi level and charge positively when above the Fermi level. At threshold, some midgap traps in the GaAs lie below the Fermi level and some lie above.  $W_-$  is the extent of the region in the GaAs in which the traps are below the Fermi level.  $W_+$  is the extent of the region in which the traps lie above the Fermi level.

We assume that the decrease in the net charge in the AlGaAs layer due to charging of the neutron-induced traps may be effectively characterized as the removal of carriers. To first order carrier removal has been shown to be linear with neutron fluence.<sup>14</sup> Therefore, the net charge in the doped AlGaAs layer after neutron irradiation may be written as

$$N_d' = N_d - a_d \phi \quad (13)$$

where

$a_d$  = the carrier removal rate in the AlGaAs

$\phi$  = the neutron fluence.

In a more detailed treatment of the charging of amphoteric traps, the carrier removal rate,  $a_d$ , is calculated by accounting for the population statistics of these traps and averaging the charge over the extent of the AlGaAs. As we intend to treat the carrier removal rate as an experimentally determined parameter, we will dispense with such detail.

At threshold it is possible that some of the amphoteric traps in the GaAs layer lie below the Fermi level and that some lie above the Fermi level. We assume that in each region the net charge is linearly dependent on the neutron fluence, to first order. In keeping with the depletion layer approximation the net charge density in the GaAs is then

$$N_- = N_a + a_- \phi; (d+a) < z < (W_- + d+a) \quad (14)$$

$$N_+ = N_a - a_+ \phi; (W_- + d+a) < z < (W_+ + W_- + d+a) \quad (15)$$

where

$a_-$  = is the effective acceptor introduction rate in the GaAs

$a_+$  = is the effective carrier removal rate in the GaAs

and

$W_-$  = the region in the GaAs in which the traps lie below the Fermi level and therefore charge negatively

$W_+$  = the region in which the traps lie above the Fermi level and therefore charge positively.

## B. TRESHOLD VOLTAGE SHIFT

Given the post-irradiation charge density in the AlGaAs layer,  $N_d'$ , the voltage drop across this layer is

$$V_{Al}' = -qN_d'd^2/2\epsilon \quad (16)$$

by analogy with Eq. (3). The difference between Eqs. (16) and (3) yields the threshold shift due to the AlGaAs layer:

$$\Delta V_{Al} = qa_d\phi d^2/2. \quad (17)$$

It should be pointed out that we have ignored charging of the traps in the spacer layer to derive the result of Eq. (17). The contribution to the threshold voltage shift due to the spacer layer is about 7% of that determined from Eq. (17). It will be shown later that the AlGaAs contribution to the threshold voltage shift is less than 3% of the total, therefore the spacer layer contribution is negligible ( $\ll 1\%$ ). The possibility that some traps in the AlGaAs might lie above midgap, and charge positively, has also been ignored. This phenomenon would tend to lessen the contribution to the threshold voltage shift from the AlGaAs layer even more because the net neutron-induced charge across the AlGaAs layer would be smaller. Because the carrier removal rate,  $a_d$ , is determined by electrical measurements, these factors (spacer layer charging and positive neutron-induced charges in the AlGaAs layer) are implicitly accounted for.

Application of Gauss's law from the interface into the bulk of the GaAs with the post-irradiation charge densities yields

$$E_i'' = (q/\epsilon)[(N_a + a_-\phi)W_- + (N_a - a_+\phi)W_+] \quad (18)$$

for the field at the interface. As written in Eq. (18), the contribution to the field at the interface due to the channel charge has been ignored. At threshold the contribution to the field by the channel charge is of the order  $z_{ave}/W_-$ . The channel charge width,  $z_{ave}$ , is on the order of 10 nm



and the depletion layer width,  $W_-$ , is on the order of 1  $\mu\text{m}$ . Therefore, contributions of order  $z_{\text{ave}}/W_-$  may be dropped. The pre-irradiation interface field may be calculated to give

$$E_i = (q/\epsilon)N_a W. \quad (19)$$

The difference between Eqs. (19) and (18) times the AlGaAs layer thickness,  $(d+a)$ , yields the neutron-induced threshold voltage shift due to the redistribution of charge in the GaAs layer.

Deep in the GaAs layer, after neutron irradiation, the charge density is given by the second term in Eq. (18) as

$$\sigma_+ = (N_a - a_+\phi)W_+. \quad (20)$$

At high fluences the neutron-induced positive charge buildup reduces the net charge in the  $W_+$  layer. Therefore, the field contribution of the charges in the  $W_+$  layer relative to the contribution due to the buildup of negative charges in the  $W_-$  is reduced. Later, we show that the threshold voltage shift in MODFETs is not appreciable for low fluences ( $<10^{13} \text{ cm}^{-2}$ ). Therefore, we shall ignore the contribution to the field at the interface due to the charges in the  $W_+$  region. The change in the field at the interface may be written as

$$\Delta E_i = (q/e)[(N_a + a_-\phi)W_- - N_a W]. \quad (21)$$

Because the effective acceptor introduction rate,  $a_-$ , will be treated as an experimentally determined parameter as long as the net charge buildup in the GaAs is negative, Eq. (21) may be used to describe the change in the field at the interface due to the neutron induced charge redistribution.

After irradiation the Fermi level,  $E_f''$ , may be determined from Eq. (5) by evaluating the post-irradiation threshold channel charge density,  $n_{\text{th}}'$ , using the post-irradiation effective charge density,  $N_-$ , and substituting

into Eq. (5). Subtracting the pre-irradiation Fermi level from the post-irradiation level and ignoring terms of order  $z_{ave}/W_-$  yields

$$\Delta E_f = (kT/3q) \ln[(1 + a_- \phi / N_a)^2 W / W_-] \quad (22)$$

for the Fermi level contribution to the neutron-induced threshold voltage shift.

In order to fully describe the neutron-induced threshold voltage shift, it remains to determine  $W_-$  in terms of GaAs parameters. Application of Gauss's law from the interface into the bulk of the GaAs yields the following for the change in potential from the interface to the edge of the  $W_-$  region:

$$V_i - V_- = (q/\epsilon) [(N_a + a_- \phi) W_-^2 / 2 + (N_a - a_+ \phi) W_+ W_-]. \quad (23)$$

Ignoring the net charge in the  $W_+$  region compared to the charge in the  $W_-$  region as discussed earlier, the width of the  $W_-$  region may be determined as

$$W_- = [2\epsilon(V_i - V_-) / q(N_a + a_- \phi)]^{1/2}. \quad (24)$$

As seen in Fig. 2, the potential change across the  $W_-$  region may be written as

$$V_i - V_- = E_g / 2 - E_f''. \quad (25)$$

Because the neutron-induced change in the Fermi level is small compared to  $E_g/2$ , this may be approximated by

$$V_i - V_- = E_g / 2 - E_f. \quad (26)$$

Substitution of Eqs. (24) and (26) into Eq. (21) and using the earlier results for the depletion layer,  $W$ , yields the neutron-induced threshold

voltage shift as a function of pre-irradiation material parameters, geometry, the effective acceptor introduction rate, the carrier removal rate, and the neutron fluence.

### C. LOW FLUENCE EXPANSION

Due to the cumbersome nonlinear dependence of the threshold voltage shift on neutron fluence, a discussion of the relative importance of each term in Eq. (21) in the low fluence limit is warranted. Expanding the neutron-induced threshold voltage in a Maclaurin series for small fluence, such that  $a_-\phi/N_a \ll 1$ , and keeping first order terms only, the threshold voltage shift may be written as

$$\Delta V_{th} = \Delta V'_{Ga} \phi [1 + (-V_{Al}/\Delta V'_{Ga})(a_- N_d/N_a^2)] \quad (27)$$

where  $V_{Al}$  is given by Eq. (3) and  $\Delta V'_{Ga}$  depends on GaAs material parameters in the following way:

$$\Delta V'_{Ga} = [(d + a) d\Delta E_i/d\phi + d\Delta E_f/d\phi] \phi = 0 \quad (28)$$

where

$$[d\Delta E_i/d\phi] \phi = 0 = (q/\epsilon) a_- [W_-] \phi = 0 \quad (29)$$

$$[d\Delta E_f/d\phi] \phi = 0 = (5kT/6q)(a_-/N_a). \quad (30)$$

For typical MODFET geometries ( $< 500 \text{ \AA}$  AlGaAs), assuming that the effective acceptor introduction rate and the carrier removal rate are of the same order (to be justified in Section III), and that the unintentional acceptor doping is much less than the AlGaAs(n) doping (a ratio of  $\sim 10^{-4}$  is typical), the AlGaAs contribution to the neutron-induced threshold voltage shift is of the order of 1%. This low fluence expansion applies to fluences of less than  $5 \times 10^{13} \text{ cm}^{-2}$ . However, the trend of GaAs dominance of the neutron degradation continues to fluences well above  $1 \times 10^{15} \text{ cm}^{-2}$  as shown in Section III.

### III. EXPERIMENTAL COMPARISON

MODFETs were fabricated on commercially-obtained, MBE grown, epitaxial material. The epilayers consisted of 1  $\mu\text{m}$  unintentionally doped GaAs, 20  $\text{\AA}$  unintentionally doped  $\text{Al}_{0.25}\text{Ga}_{0.75}\text{As}$ , 500  $\text{\AA}$  n- $\text{Al}_{0.25}\text{Ga}_{0.75}\text{As}$  ( $n = 1 \times 10^{18} \text{ cm}^{-3} \text{ Si}$ ), and 200  $\text{\AA}$  n-GaAs ( $n = 1 \times 10^{18} \text{ cm}^{-3} \text{ Si}$ ). The aluminum mole fraction of  $x = 0.25$  was chosen to minimize complications from high concentrations of pre-irradiation deep levels characteristic of higher mole fraction alloys. A standard mesa isolation gate process was used to define the transistors. Figure 3 shows a stylized cross section of the devices fabricated for this study.

Using an unintentional acceptor doping density,  $N_a$ , of  $5 \times 10^{14} \text{ cm}^{-3}$ ,  $\text{AlGaAs}(n)$  doping,  $N_d$ , of  $1 \times 10^{18} \text{ cm}^{-3}$ , a post-processed doped  $\text{AlGaAs}$  layer thickness,  $d$ , of 400  $\text{\AA}$ , and a spacer layer thickness,  $a$ , of 20  $\text{\AA}$  our threshold voltage analysis, yields a value of  $-.620$  volts for the pre-irradiation threshold voltage. This is in reasonable agreement with our measured values which range from  $-.41$  to  $-.73$  volts. Variation in the measured values is a result of variations in the thickness of the  $\text{AlGaAs}$  arising from non-uniform processing. The value used for analysis, 420  $\text{\AA}$ , is a nominal value and gives rise to the discrepancy between our calculated value and the measured values.

The devices were exposed to neutron fluences ranging from  $5 \times 10^{13} \text{ cm}^{-2}$  to  $1 \times 10^{15} \text{ cm}^{-2}$  in the SPR-III nuclear reactor at Sandia National Laboratories. Shown in Table 1 are the measured threshold voltage shifts for the Aerospace fabricated MODFETs. The nominal device parameters are those cited above. In Fig. 4 the data for the measured threshold voltage shift from Table 1 is plotted versus neutron fluence. Also shown in Fig. 4 are the modeling results for the threshold voltage change, assuming an  $\text{AlGaAs}$  carrier removal rate,  $a_d$ , of  $10 \text{ cm}^{-1}$  and a GaAs acceptor introduction rate,  $a_-$ , of  $3 \text{ cm}^{-1}$ . The solid curve in Fig. 4 is the modeling result of the full model, channel charge and  $\text{AlGaAs}$  layer contribution included, while the dashed curve is the result obtained by making the simplifying assumptions discussed earlier and ignoring the  $\text{AlGaAs}$  contribution.

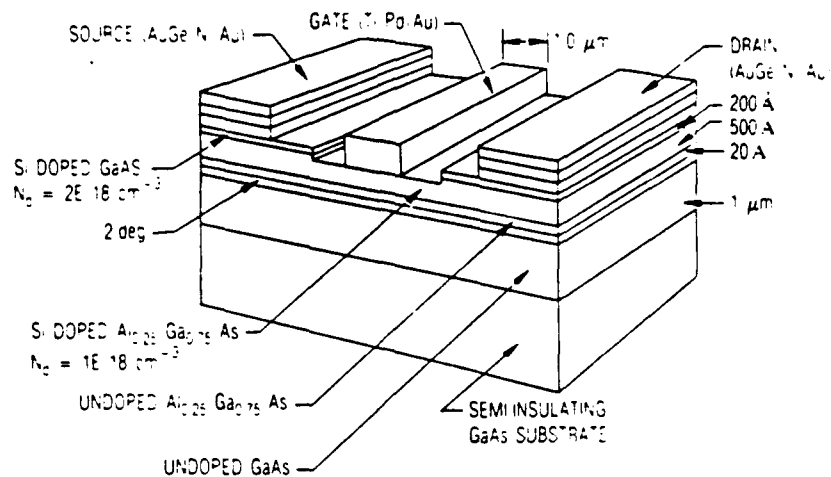


Fig. 3. Stylized Version of the MODFET Structure Used in This Study. Low mole fraction AlGaAs was used to avoid deep pre-irradiation electron traps.

Table 1. Measured Threshold Voltage Shifts of Aerospace Fabricated MODFETS

Neutron Fluence	Threshold Shifts (Volts)
9.2E + 14	0.1864 ± 0.0214
4.9E + 14	0.1100 ± 0.0100
2.2E + 14	0.0540 ± 0.0150
1.0E + 14	0.0319 ± 0.0155
5.1E + 13	0.0184 ± 0.0059

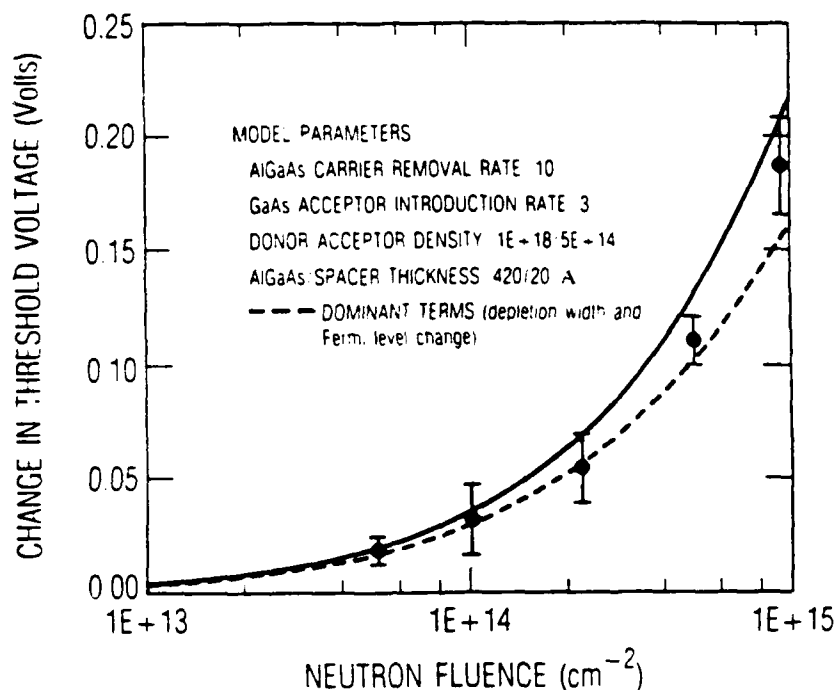


Fig. 4. Change in Threshold Voltage vs Neutron Fluence for the Model Parameters Shown

For these values of  $a_d$  and  $a_-$ , the agreement between the model and the experiment is very good over the whole range. The value of  $a_d$  was chosen from the literature<sup>14</sup> and verified by Hall measurement, then  $a_-$  was used to fit the data. Only at the highest fluence levels,  $\sim 5 \times 10^{14} \text{ cm}^{-2}$ , do the simplified model results diverge significantly from the full model results. The modeling results for the threshold voltage using these parameters are shown in Fig. 5. The increase in the threshold voltage with neutron fluence is very similar to the increase in threshold voltage due to increased acceptor doping, discussed elsewhere.<sup>5</sup>

Shown in Fig. 6. are the contributions of each term described in Eq. (11). The threshold voltage shift data and modeling results of Fig. 4 are included. The change in the Fermi level,  $\Delta E_f$ , and the change in the field at the interface to the redistribution of charge in the GaAs,  $E_i$ , dominate and are almost equal, whereas the AlGaAs contribution is about 2.5% over the whole range of neutron fluence.

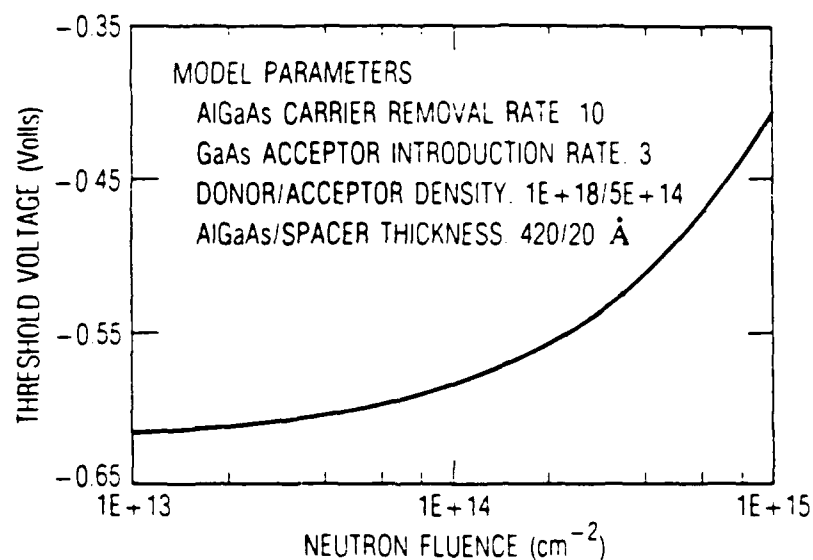


Fig. 5. Threshold Voltage vs Neutron Fluence Using the Model Parameters Used to Fit the Threshold Shift Data

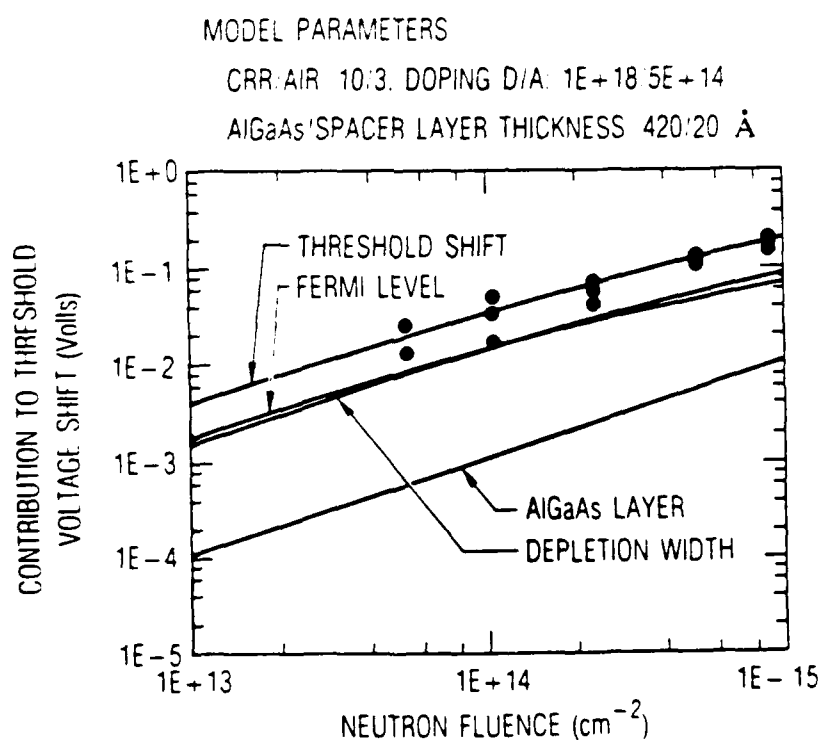


Fig. 6. Contributions to the Threshold Voltage Shift vs Neutron Fluence

#### IV. DISCUSSION

In Fig. 7 we have shown a diagram of the conduction band of the AlGaAs/ GaAs interface of a typical MODFET structure at threshold as the neutron fluence varies. Also shown are the positions of the Fermi energy and the first energy level in the 2-D well as the fluence increases from some initial value, (i), to some final value, (f). As the neutron fluence increases, the Fermi level shifts upward closer to the bottom of the well and the first energy level moves up away from the bottom of the well. The difference between the Fermi level and the first quantum level determines the amount of charge in the channel. In keeping with the definition of threshold, the channel charge must increase as the effective charge density near the interface increases with neutron fluence as the midgap traps near the interface charge negatively.

As the charge in the channel increases, the field at the interface increases and the 2-D well width decreases, consistent with the increase in the energy level. At the same time the depletion width is decreasing. Since the depletion width contribution to the threshold voltage shift depends on the product of the depletion width and the effective acceptor density, an increasing depletion contribution means that the increase in the effective acceptor density must dominate.

For the device parameters cited above, we have plotted the Fermi energy and first quantum well energy level, the change in the Fermi energy and the change in the first quantum level, and the depletion width as a function of neutron fluence in Figs. 8, 9, and 10 respectively. Figure 8 shows that both the Fermi level and the first quantum level increase with neutron fluence. The Fermi level increases more than the first energy level, as shown in Fig. 9, increasing the amount of charge in the channel. Shown in Fig. 10 is a three-fold decrease in the depletion width from a fluence of  $1 \times 10^{13}$  to  $1 \times 10^{15} \text{ cm}^{-2}$ .



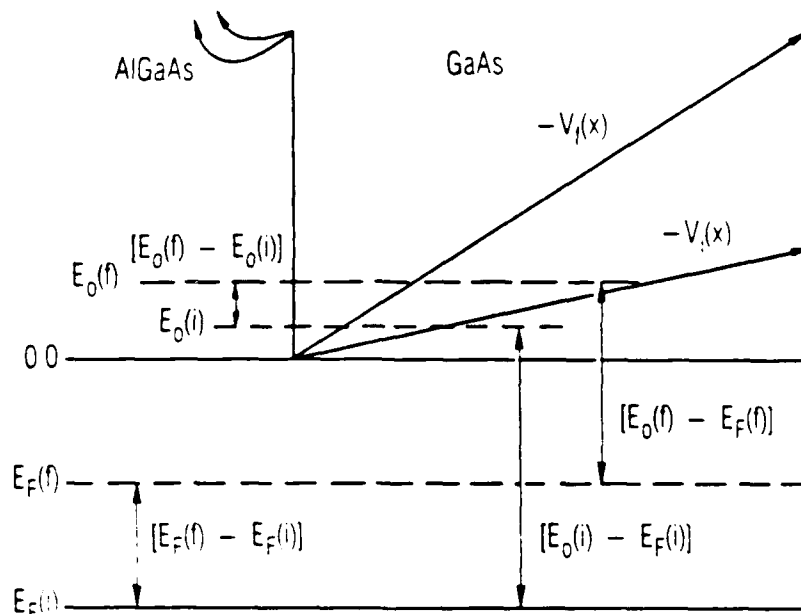


Fig. 7. MODFET Energy Bands Near the Interface Pre-(i) and Post-(f) Neutron Irradiation

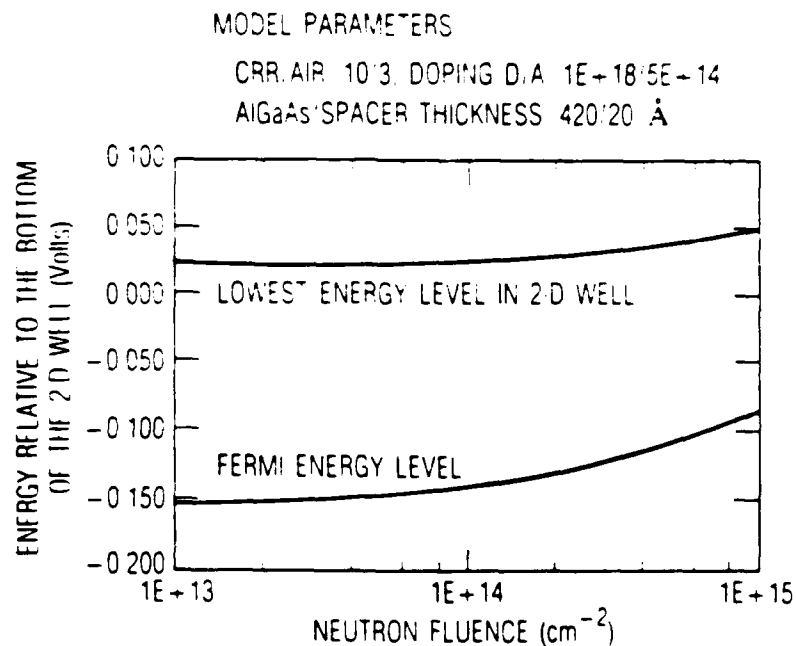


Fig. 8. Energy of the Quantum Well Level and the Fermi Level vs Neutron Fluence

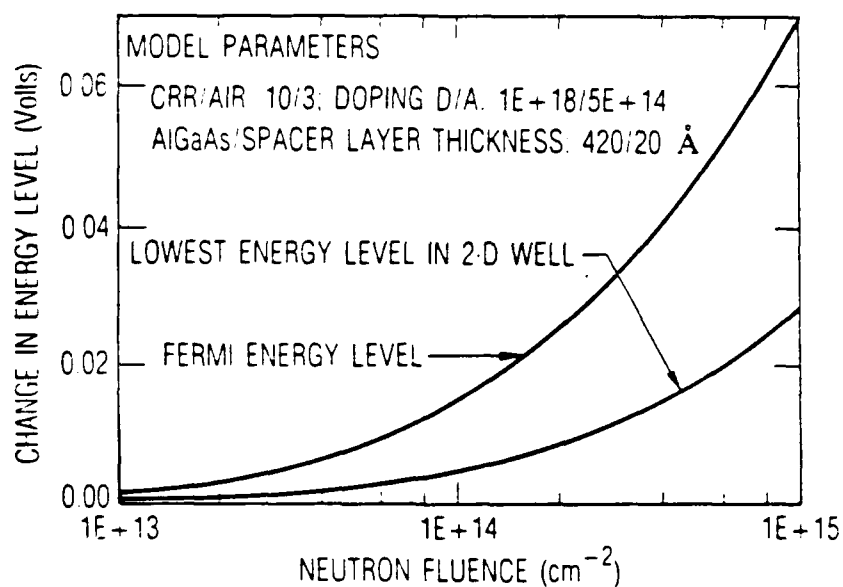


Fig. 9. Change in the Quantum Well Level and the Fermi Level vs Neutron Fluence

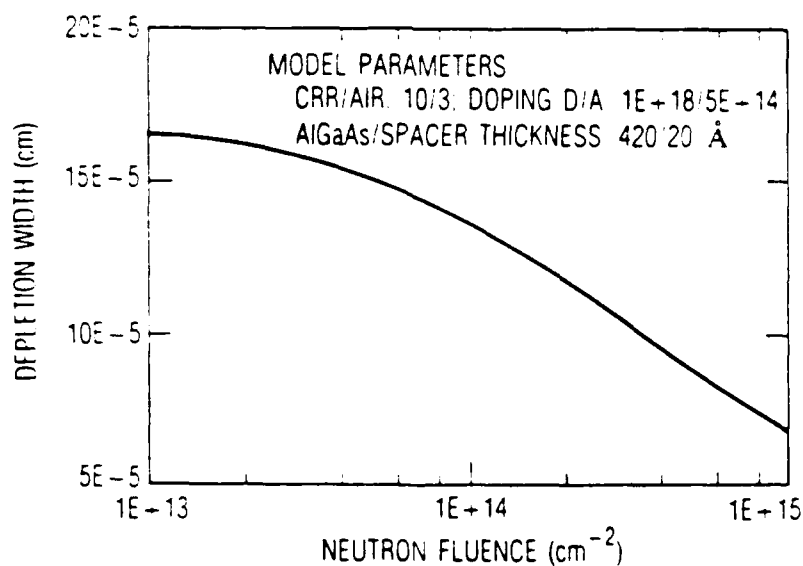


Fig. 10. Depletion Layer Width vs Neutron Fluence

## V. SUMMARY

We have developed and presented a finite temperature, charge control model for the threshold voltage of modulation-doped field effect transistors which includes degradation due to neutrons. The model has been applied to Aerospace fabricated AlGaAs/GaAs MODFETs which have been exposed to neutron fluences from  $5 \times 10^{13}$  to  $1 \times 10^{15} \text{ cm}^{-2}$ . Our analysis shows that the degradation of the threshold voltage is due primarily to a redistribution of charge in the GaAs rather than degradation in the AlGaAs. This implies that the GaAs doping density in the depletion layer is an important factor in determining neutron hardness of MODFETs. Assuming a constant acceptor introduction rate, higher doping in the GaAs will make these structures harder to neutrons.

## REFERENCES

1. R. Dingle, M. D. Feuer, and C. W. Tu, "The Selectively Doped Heterostructure Transistor: Materials, Devices, and Circuits," in VLSI Electronics: Microstructure Science, edited by N. G. Einspruch and W. R. Wisseman (Academic Press, N.Y. 1985), Chapter 6.
2. P. M. Solomon and H. Morkoc, "Modulation-Doped GaAs/AlGaAs Heterojunction Field-Effect Transistors (MODFETs), Ultrahigh-Speed Device for Supercomputers," IEEE Trans. Electron Devices, ED-31, 1015-1027 (Aug. 1984).
3. M. Abe et al. "GaAs VLSI Technology for High-Speed Computers," in VLSI Electronics: Microstructure Science, edited by N. G. Einspruch and W. R. Wisseman (Academic Press, N.Y. 1985), Chapter 9.
4. M. N. Yoder, "Military Applications of GaAs Integrated Circuits," in VLSI Electronics: Microstructure Science, edited by N. G. Einspruch and W. R. Wisseman (Academic Press, N.Y. 1985), Chapter 10.
5. R. J. Krantz and W. L. Bloss, "Strong Inversion Model of Threshold Voltage in Modulation Doped Field Effect Transistors: The Role of Unintentional Acceptors," and references therein. Submitted to IEEE Trans. Electron Devices.
6. D. Delagebeaudeuf and N. T. Linh, "Metal-(n)AlGaAs-GaAs Two-Dimensional Electron Gas FET," IEEE Trans. Electron Devices, ED-29, 955-960, (June 1982).
7. H. L. Stormer, "Electron Mobilities in Modulation-Doped GaAs-(AlGa)As Heterostructures," Surface Science, 132, 519-526, (1983).
8. L. W. Aukerman, "Radiation-Produced Energy Levels in Compound Semiconductors," J. Appl. Phys. 30, 1239-1243, (Aug. 1959).
9. L. W. Aukerman, "Radiation Effects," in Semiconductors and Semimetals: Physics of III-V Compounds, edited by R. K. Willardson and A. C. Beer (Academic Press, N.Y. 1968), Chapter 6.
10. R. K. Willardson, "Transport Properties in Silicon and Gallium Arsenide," J. Appl. Phys. 30, 1158-1165, (Aug. 1959).
11. J. R. Crawford, Jr. and J. W. Cleland, "Nature of Bombardment Damage and Energy Levels in Semiconductors," J. Appl. Phys. 30, 1204-1213, (Aug. 1959).

12. V. C. Burkig, J. L. McNichols, and W. S. Ginell, "Infrared Absorption in Neutron-Irradiated GaAs," J. Appl. Phys. 40, 3268-3273, (July 1969).
13. H. J. Stein, "Electrical Studies of Low-Temperature Neutron- and Electron-Irradiated Epitaxial n-type GaAs," J. Appl. Phys. 40, 5300-5307, (Dec. 1969).
14. R. Zuleeg, "Radiation Effects in GaAs Integrated Circuits," in VLSI Electronics: Microstructure Science, edited by N. G. Einspruch and W. R. Wisseman (Academic Press, New York 1985), Chapter 11 and references therein.

## APPENDIX A - (Fermi Level and $n_s$ )

In a 2-D electron gas, the energy of an electron in the  $i$ th band is given by:

$$E_i = E_{i0} + \hbar^2 k^2 / 2m_1 \quad (A1)$$

where

- $\hbar$  = the Planck constant divided by  $2\pi$
- $k$  = the longitudinal wavevector
- $m_1$  = the longitudinal effective mass of the carriers
- $E_{i0}$  = the  $k = 0$  energy level of the quantum well.

The concentration of carriers is calculated by evaluating the following:

$$n_s = g_s (1/A) \sum_i \int_{E_{i0}}^{\infty} g(E_i) f(E_i) dE_i \quad (A2)$$

where

- $g_s$  = the spin degeneracy of the carriers
- $g(E_i)$  = density of states
- $A$  = device area
- $f(E_i)$  = Fermi-Dirac distribution function
- $\sum_i$  = the sum over 2-D energy levels.

Equation (A2) may be evaluated by considering that:

$$g(E_i) = g(k) dk \quad (A3a)$$

where

$$g(k)dk = dA_k/A_k \quad (A3b)$$

and

$$A_k = \pi k^2: \text{the area in reciprocal space } [(2\pi)^2/A]. \quad (A3c)$$

Using Eqs. (A1) and (A3), Eq. (A2) takes the following form:

$$n_s = (g_s m_1 / 2\pi M^2) \sum_i \int_{E_{i0}}^{\infty} \{1 + \exp[(E - E_f)/kT]\} dE. \quad (A4)$$

Effecting the integration in Eq. (A4), assuming only one energy level,  $E_0$ , and using the spin degeneracy factor,  $g_s$ , for electrons ( $g_s = 2$ ) the Fermi energy may be calculated:

$$E_f = E_0 + (kT) \ln[\exp(\pi M^2 n_s / (m_1 kT)) - 1]. \quad (A5)$$

Near-threshold  $n_s$  is small and the exponential may be expanded. Conversion to potential units then results in Eq. (5) in the text.

# APPENDIX B - ( $E_0$ and $n_s$ )

The first quantum level may be calculated in the triangular well approximation using a normalized variational envelope wave function:

$$\phi_0 = (b^3/2)^{1/2} z(e^{-bz/2}) \quad (B1)$$

where  $b$  is a variational parameter to be determined. The Hamiltonian for the triangular well is:

$$H = -(\hbar^2/2m_1)d^2/dz^2 + qV(z) \quad (B2a)$$

where

$$V(z) = E_1 z: z > 0 \quad (B2b)$$

$$V(z) = \text{infinity}: z < 0 \quad (B2c)$$

$\hbar$  = the Planck constant divided by  $2\pi$

$m_1$  = longitudinal effective mass of the carriers.

Minimizing the energy,  $\langle \phi_0 | H | \phi_0 \rangle$  with respect to  $b$  yields:

$$b = [4Em_1 q/\hbar^2]^{1/3} \quad (B3)$$

where

$E$  = the field in the potential well.



The first energy level may be calculated by evaluating the following:

$$E_0 = \langle \phi_0 | H | \phi_0 \rangle \quad (B4a)$$

which yields:

$$E_0 = (9\hbar^2/8m_1q)(4Em_1q/\hbar^2)^{2/3}. \quad (B4b)$$

Application of Gauss's law from the interface into the bulk of the structure shown in Fig. 1 gives the field at the interface:

$$E = (q/\epsilon)(n_s + N_a W). \quad (B5)$$

Substitution of Eq. (B5) into Eq. (B4b) yields Eq. (6) in the text where:

$$C_1 = (9\hbar^2/8m_1q)(4qm_1q^2/\hbar^2\epsilon)^{2/3}.$$

# APPENDIX C - ( $n_{th}$ , $N_a$ , and $W$ )

Assuming the criteria for threshold as stated in the text:

$$n_{th} = N_a z_{ave} \quad (C1)$$

where

$N_a$  = the acceptor density

$z_{ave}$  = the average position of carriers in the 2-D well.

The average position may be calculated in the triangular well approximation using the variational wave function from Appendix B. Thus:

$$z_{ave} = \langle \phi_0 | z | \phi_0 \rangle \quad (C2a)$$

which reduces to:

$$z_{ave} = 3/b \quad (C2b)$$

where the variational parameter,  $b$ , is given in Appendix B. Combining Eqs. (C1) to (C3) and substituting for  $b$  yields:

$$z_{ave} = N_a [27W^2/4Em_1q]^{1/3} \quad (C3)$$

where

$E$  = is the field in the potential well.

At threshold the field is dominated by the depletion layer charge and may be approximated as:

$$E = qN_a W / \epsilon \quad (C4)$$

where

$W$  = the depletion layer width.

Substitution of Eqs. (C4) and (C3) into Eq. (C1) yields Eq. (8) used in the text.

## LABORATORY OPERATIONS

The Aerospace Corporation functions as an "architect-engineer" for national security projects, specializing in advanced military space systems. Providing research support, the corporation's Laboratory Operations conducts experimental and theoretical investigations that focus on the application of scientific and technical advances to such systems. Vital to the success of these investigations is the technical staff's wide-ranging expertise and its ability to stay current with new developments. This expertise is enhanced by a research program aimed at dealing with the many problems associated with rapidly evolving space systems. Contributing their capabilities to the research effort are these individual laboratories:

Aerophysics Laboratory: Launch vehicle and reentry fluid mechanics, heat transfer and flight dynamics; chemical and electric propulsion, propellant chemistry, chemical dynamics, environmental chemistry, trace detection; spacecraft structural mechanics, contamination, thermal and structural control; high temperature thermomechanics, gas kinetics and radiation; cw and pulsed chemical and excimer laser development including chemical kinetics, spectroscopy, optical resonators, beam control, atmospheric propagation, laser effects and countermeasures.

Chemistry and Physics Laboratory: Atmospheric chemical reactions, atmospheric optics, light scattering, state-specific chemical reactions and radiative signatures of missile plumes, sensor out-of-field-of-view rejection, applied laser spectroscopy, laser chemistry, laser optoelectronics, solar cell physics, battery electrochemistry, space vacuum and radiation effects on materials, lubrication and surface phenomena, thermionic emission, photo-sensitive materials and detectors, atomic frequency standards, and environmental chemistry.

Computer Science Laboratory: Program verification, program translation, performance-sensitive system design, distributed architectures for spaceborne computers, fault-tolerant computer systems, artificial intelligence, micro-electronics applications, communication protocols, and computer security.

Electronics Research Laboratory: Microelectronics, solid-state device physics, compound semiconductors, radiation hardening; electro-optics, quantum electronics, solid-state lasers, optical propagation and communications; microwave semiconductor devices, microwave/millimeter wave measurements, diagnostics and radiometry, microwave/millimeter wave thermionic devices; atomic time and frequency standards; antennas, rf systems, electromagnetic propagation phenomena, space communication systems.

Materials Sciences Laboratory: Development of new materials: metals, alloys, ceramics, polymers and their composites, and new forms of carbon; non-destructive evaluation, component failure analysis and reliability; fracture mechanics and stress corrosion; analysis and evaluation of materials at cryogenic and elevated temperatures as well as in space and enemy-induced environments.

Space Sciences Laboratory: Magnetospheric, auroral and cosmic ray physics, wave-particle interactions, magnetospheric plasma waves; atmospheric and ionospheric physics, density and composition of the upper atmosphere, remote sensing using atmospheric radiation; solar physics, infrared astronomy, infrared signature analysis; effects of solar activity, magnetic storms and nuclear explosions on the earth's atmosphere, ionosphere and magnetosphere; effects of electromagnetic and particulate radiations on space systems; space instrumentation.